ResearchGate

See discussions, stats, and author profiles for this publication at: https://www.researchgate.net/publication/6253279

Effect of Acid−Base Equilibria on the Donnan Potential of Layer-by-Layer Redox Polyelectrolyte Multilayers

ARTICLE *in* THE JOURNAL OF PHYSICAL CHEMISTRY B · AUGUST 2007

Impact Factor: 3.3 · DOI: 10.1021/jp071867n · Source: PubMed

CITATIONS
36

READS
36

3 AUTHORS, INCLUDING:

Federico J. Williams
University of Buenos Aires
87 PUBLICATIONS **1,380** CITATIONS
SEE PROFILE

Ernesto J Calvo
University of Buenos Aires
151 PUBLICATIONS **3,911** CITATIONS
SEE PROFILE

Available from: Federico J. Williams
Retrieved on: 17 January 2016

Effect of Acid−Base Equilibria on the Donnan Potential of Layer-by-Layer Redox Polyelectrolyte Multilayers

Mario Tagliazucchi,[†] Federico J. Williams,[†,‡] and Ernesto J. Calvo*[,†]

INQUIMAE, Departamento de Química Inorgánica, Analítica y Química Física, Facultad de Ciencias Exactas y Naturales, Universidad de Buenos Aires, C1428EHA Buenos Aires, Argentina, and Department of Surface Chemistry and Coatings, Center for Industrial Research, TENARIS, Dr. Simini 250, B2804MHA Campana, Buenos Aires, Argentina

Received: March 7, 2007; In Final Form: April 26, 2007

In polymer films carrying an excess of fixed charge the electrostatic penalty to bring ions of same charge from the bathing electrolyte into the film sets a membrane potential (Donnan Potential) across the film−electrolyte interface. This potential is responsible for the ionic permselectivity observed in polyelectrolyte membranes. We have used electrochemical measurements to probe the dependence of the Donnan potential on the acid−base equilibrium in layer-by-layer self-assembled polyelectrolyte multilayers. The voltammperogram peak position of the Os(III)/Os(II) couple in self-assembled polyelectrolyte multilayers comprised of poly(allylamine) derivatized with $Os(bpy)_2PyCl^+$ and poly(vinylsulfonate) was recorded in solutions of increasing ionic strength for different assembly and testing solution pH. Protonation−deprotonation of the weak redox poly(allylamine) changes the fixed charge population in the as prepared (intrinsic) self-assembled redox polyelectrolyte multilayers. For films assembled in solutions of pH higher than the test solution pH, the Donnan plots (E_{app} vs log C) exhibit a negative slope (anionic exchanger) while for films assembled at lower pH than that of the test solution positive slopes (cationic exchanger) are apparent. The ion exchange mechanism has been supported by complementary electrochemical quartz crystal microbalance. X-ray photoelectron spectroscopy and infrared reflection−absorption spectroscopy experiments demonstrated that the as prepared films have a memory effect on their protonation state during assembly, which leads to the observed dependence of the Donnan potential on the adsorption pH.

1. Introduction

Very well characterized ultrathin films of polyelectrolytes can be built over virtually any substrate by means of the layer-by-layer self-assembly (LbL-SA) technique.[1,2] As its name indicates, the adsorption steps are self-regulating and therefore fine control over the multilayer structure, composition, and properties should be indirectly exerted by manipulation of different processing variables. Due to the high degree of ionic cross-linking in electrostatically self-assembled films,[3] it is not surprising that the most studied parameters affect the screening or neutralization of polymer-bound charged groups, namely, the ionic strength at processing[2,4−6] and, for weak polyelectrolytes, the pH of the dipping solution. Effects of the assembly pH on film thickness,[7,8] surface roughness,[7] dielectric properties,[9] and surface wettability[7,8,10] have been demonstrated.

The assembled multilayers also respond to pH changes in the outer solution due to the acid−base equilibria in the weak polyelectrolytes. Examples in the literature include swelling transitions,[11,12] pH-induced microporosity,[12] and changes in film permeability[7,13−15]

The Donnan or membrane potential is of fundamental importance in polymer science, since it governs the permselectivity of polyelectrolyte structures toward ions in the external solution. It arises from the presence of fixed ionic charge, which exclude ions of the same charge. In weak polyelectrolytes films the fixed charges are pH-dependent and therefore the acid−base equilibria may determine the Donnan permselectivity. Examples of this are the pH-dependent permeability of charged organic molecules through polyelectrolyte films[13−15] and microcapsules.[16] Also, it has been demonstrated that ionic permselectivity and permeability could be controlled by the pH during assembly and testing in photo-cross-linked LbL-SA films.[17] Cation selective pH-switchable multilayers have been constructed from photolysis of multilayers containing photo-cross-linkeable and photolabile groups.[18]

In a previous report,[19] direct measurement of the Donnan potential in multilayers built from poly(allylamine) modified with $Os(bpy)_2PyCl^+$ (PAH-Os, see inset in Figure 2) and anionic poly(vinyl sulfonate) was achieved recording the apparent redox potential of the osmium couple in electrolyte solutions. While Donnan permselectivity was shown to depend on the nature of the polyelectrolyte capping layer and the ionic strength, the influence of the solution pH during assembly and testing was not systematically studied. Here we have extended these studies to analyze the effect of the acid base equilibria on the Donnan potential of redox weak polyelectrolyte multilayers by combining electrochemical methods (cyclic voltammetry (CV) and electrochemical quartz crystal microbalance (EQCM)) with surface characterization techniques (X-ray photoelectron spectroscopy (XPS), Fourier transform infrared reflection−absorption spectroscopy (FTIR-RAS) and ellipsometry) The present study is relevant to the design of structures with specific ionic permselectivity and to aspects of supramolecular chemistry of

* Author to whom correspondence should be addressed. E-mail: calvo@qi.fcen.uba.ar.
[†] Universidad de Buenos Aires.
[‡] TENARIS.

10.1021/jp071867n CCC: $37.00 © 2007 American Chemical Society
Published on Web 06/21/2007

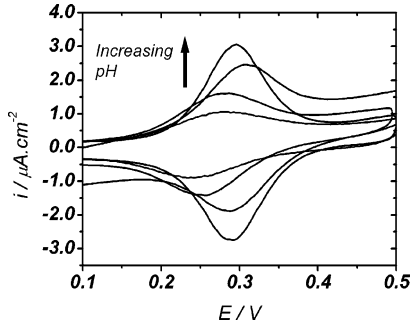

Figure 1. Cyclic voltammograms of $(PAH\text{-}Os)_4(PVS)_4PAH\text{-}Os$ multilayer modified Au electrodes self-assembled from PVS and PAH-Os solutions of different pH, 3.5, 5.5, 7.3, and 8.3, and measured in pH 7.3 solution (0.2 mM KNO_3 Tris 20 mM). Sweep rate: 0.025 V s^{-1}.

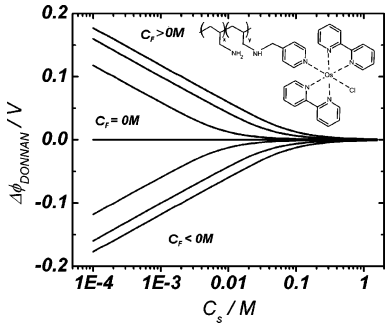

Figure 2. Donnan potential calculated with eq 5 vs C_S for different concentrations of fixed charge in PAH-Os polyelectrolyte film (from top to bottom): 0.10, 0.05, 0.01, 0, −0.01, −0.05, −0.10 M. Inset: Chemical structure of PAH-Os.

weak polyelectrolyte layer-by-layer self-assembled films such as charge balance and structure−function relationships.

2. Experimental Section

2.1. Reagents and Materials. All solutions were prepared with 18 MΩ Milli-Q (Millipore) water. The following chemicals were used without further purification: poly(acrylic acid), PAA (35% solution in water, *M*w ≈ 100 000, Aldrich); poly(sodium vinyl sulfonate), PVS (25 wt % solution in water, Aldrich); sodium 3-mecapto-propane-sulfonate, MPS (Aldrich). Chemicals employed in electrolyte solutions, glacial acetic acid, ammonium hydroxide, KNO_3, Trizma base, and TrizmaHCl, were of analytical grade and used as received.

The osmium bipyridine derivatized redox polymer $Os(bpy)_2ClPyCH_2NH$−poly(allylamine) (PAH-Os) was synthesized as previously reported.[20] Thiol solutions of 20 mM 3-mercapto-1-propane-sulfonic acid (MPS) (Aldrich) in 10 mM sulfuric acid (Merck) were prepared before each experiment in order to avoid oxidation in air. No salt was added to polyelectrolyte solutions. The pH of the PAH-Os, PVS, and PAA solutions was adjusted employing 0.1 M solutions of HCl or NaOH respectively.

2.2. Surface Modification. Silicon (100) substrates were coated with 200 nm gold layer on a 20 nm titanium and 20 nm palladium adhesion layer by thermal evaporation with an Edwards Auto 306 vacuum coating system at $P < 1 \times 10^{-8}$ bar and employed as electrodes.

Alternatively, 10 MHz Au-coated 14 mm in diameter and 0.168 mm in thickness AT-cut quartz crystals with an active area of 0.196 cm^2 (International Crystal Manufacturing Company, Inc., Oklahoma City, OK, catalogue no. 31210) were employed for EQCM measurements.

In the first step, the gold film substrates were primed with sulfonate groups by immersion in an MPS solution for 30 min followed by rinsing with deionized water. After thiol adsorption, the first polycation layer was deposited on thiol-modified Au surface by immersion in PAH-Os solution for 15 min, followed by thoroughly rinsing with Milli-Q water. The next and subsequent layers were deposited onto the modified surface by alternate immersion in a solution of the respective polyanion (PVS or PAA) or polycation (PAH-Os) for 15 min and rinsing with Milli-Q water until the desired number of layers was achieved. The adsorption times were previously determined by ellipsometric transient measurements and EQCM.[21]

2.3. Electrochemical Experiments. Cyclic voltammetry measurements were carried out at room temperature with an Autolab PGSTAT 30 potentiostat (Autolab, Ecochemie, Holland). All experiments were performed in a purpose built three-electrode Teflon cell, with an electrode exposed area of approximately 0.25 cm^2 delimited by an inert O-ring.

A Ag/AgCl electrode (3 M KCl (0.210 V vs NHE)) was employed as the reference electrode, and all electrode potentials herein are quoted with respect to it; a platinum gauze auxiliary electrode of large area was employed. Before thiol adsorption the electrode potential was cycled in 2 M sulfuric acid between 0.2 and 1.6 V at 0.1 V s^{-1} to check for surface contamination, and electrochemically active areas were calculated from the reduction peak of gold oxide.[22]

2.4. Electrochemical Quartz Crystal Microbalance. The quartz crystal resonator at 10 MHz was used as a QCM ,which has been described elsewhere.[23] The crystals were mounted in the cells by means of viton O-ring seals, with only one face in contact with the electrolyte; this electrode was a common ground to both the AC and DC circuits. Previous results for the system PAH-Os/PVS have shown that this film could be considered as acoustically thin,[24] and therefore frequency shifts have been directly transformed into mass changes by employing the Sauerbrey equation.

2.5. Ellipsometry. For ellipsometric measurements a Sentech variable angle rotating analyzer automatic ellipsometer (vertical type, 2000 FT model) equipped with a 632.8 nm laser as polarized light source was employed. All measurements were performed at an incidence angle of 70.00°. All adsorption steps were carried out avoiding any variations of the electrode position in order to keep the system alignment. Ellipsometric parameters variations lower than the data dispersion for a single measurement (0.01 in ψ and 0.05 in Δ) were guaranteed in this way.

Ellipsometric angles ψ and Δ were determined from reflection-induced changes in the state of polarization of linearly polarized light; these were related to the ellipsometric ratio ρ

$$\rho = \tan(\psi)\exp(i\Delta) = \frac{r_p}{r_s}$$

where tan ψ represents the amplitude change in ρ, Δ is the phase difference change, and r_p and r_s are the complex reflection coefficients for light polarized parallel and perpendicular to the plane of incidence, which depend on the structure and optical properties of the system.

After each adsorption step, the sample was rinsed with Milli-Q water and dried with N_2. Then, the ellipsometric parameters, ψ and Δ, were collected manually. The experimental data were fitted as described elsewhere.[25]

2.6. FTIR-RAS Experiments. Infrared spectra were recorded using a Nicolet Magna 560 FTIR spectrometer with an MCT-A cryogenic detector. Reflection absorption spectroscopy was

measured as described elsewhere[26] with a 4 cm^{-1} spectral resolution integrating 100 interferogram scans.

2.7. XPS Experiments. XPS measurements were performed using a commercial XPS system (Specs SAGE 150) equipped with a dual-anode Mg/Al X-ray source and an hemispherical electron energy analyzer. The reported binding energies (BEs) are based on the analyzer energy calibration using reference samples (Ag $3d_{5/2}$ and Au $4f_{7/2}$). No charge compensation was necessary and no differential charging features were observed (e.g., low BE tails) given that we have measured sufficiently thin films on grounded conducting substrates. Atomic ratios were calculated from the integrated intensities of core levels after instrumental and photoionization cross-section corrections.[27]

3. Results and Discussion

3.1. Determination of the Donnan Potential from the Os(II)/Os(III) Apparent Redox Potential. The effect of the acid−base equilibria on the electrochemical response of redox multilayers assembled from solutions of different pH in the range 3.5 to 8.3 was probed by cyclic voltammetry. For each assembly pH condition, two films that differ in the nature of the capping layer were built: $(PAH\text{-}Os)_4(PVS)_4PAH\text{-}Os$ (positively charged PAH-Os capping layer) and $(PAH\text{-}Os)_5(PVS)_5$ (negatively charged PVS capping layer).

Figure 1 shows voltammograms recorded for $(PAH\text{-}Os)_4(PVS)_4PAH\text{-}Os$ electrodes built from solutions of different pH. Several general trends can be observed in the voltammetric waves of the osmium pyridine−bipyridine complex:

(i) The area under the peaks increases the higher the pH of redox polymer solutions; thus the total amount of adsorbed polymer increases at higher pH. This will be discussed in section 3.4: Effect of the Assembly pH on Film Thickness.

(ii) There is a slight increase in the separation between the oxidation and reduction peaks with the decrease of the adsorption pH, from an almost zero value (ideal surface reversible system) at pH 8.3 to approximately 34 mV at pH 3.5. The same behavior has been previously reported for PAH-Os/glucose oxidase (GOx) multilayers[28] and has been ascribed to a hindrance in charge transport for films assembled at low pH, because they have a more compact structure than those built at higher pH and therefore have more restricted segmental motions and less mobile redox centers.

(iii) The peak position shifts toward higher potential values the higher the adsorption pH. This has been been explained by Anson[29,30] and Doblhofer[31,32] as resulting from a Donnan or membrane potential between the electrolyte and the film.[19]

The shift in apparent redox potential ($E_{app}^{1/2}$) is equal to the interfacial electrical potential that arises due to the different ionic composition inside the film and in the electrolyte

$$E_{app}^{1/2} = E^0 + \Delta\phi_D \tag{1}$$

where E^0 is the formal redox potential of the Os(II)/Os(III) complex in the absence of electrostatic work terms due to the charged polymer film, i.e., in solution, and $\Delta\phi_D$ is the interfacial Donnan potential, which is related to the presence of pH-dependent fixed charges in the film. In the treatment above we have neglected the small correction for liquid junction potential.[33,34]

Assuming for simplicity that there is no change in the resolvation energy of the exchanged ions in the solution and inside the film, that they have the same activity coefficients and neglecting the effect of the solution ionic strength and the redox state of the film on the concentration of fixed charges, $\Delta\phi_D$ can be calculated with[19,32]

$$\Delta\phi_D = \frac{RT}{F}\ln\left[\frac{C_F + (C_F^{\,2} + 4C_S^{\,2})^{1/2}}{2C_S}\right] \tag{2}$$

where C_S is the 1:1 electrolyte concentration in the external solution and C_F is the concentration of fixed charged sites in the polymer and can be positive/negative for films bearing fixed positive/negative fixed ionic charges. A detailed derivation of eq 2 has been included in the Supporting Information. It should be noted that the difference with eq 1 in ref 19 where C_F was strictly positive and the sign of the fixed charges was accounted for the parameter ω, while in the present analysis C_F can be either positive or negative.

For $C_S \ll C_F$, Donnan preselectivity applies and eq 2 is simplified to

$$\Delta\phi_D \cong \omega\frac{RT}{F}\ln\left(\frac{C_F}{C_S}\right) \tag{3}$$

where $\omega = +1$ for anion exchange and positive charge in the polyelectrolyte, and conversely $\omega = -1$, C_F refers here to the analytical concentration of charges or $|C_F|$. Equation 3 has been used in the seminal work of Naegeli et al.[29] to explain Donnan effects for Nafion coated electrodes, but it does not account for Donnan breakdown at $C_S \geq C_F$ while eq 2 does.

Equation 2 strictly refers to the ionic equilibrium between two phases: (i) a thick membrane carrying a number of fixed charges and (ii) an external electrolyte. For thinner membranes, i.e., membranes with a surface charge and thickness $d \rightarrow 1/\kappa_{DH}$ (κ_{DH} is the Debye−Hückel parameter of the surface charge) the Donnan potential leads to the surface potential.[35] In the present work we have studied multilayer films with $d \geq 6$ nm, and the analysis was carried out with the standard Donnan model.

For ampholytic films (such as LbL multilayers) C_F should be regarded as the difference between the concentration of positive and negative fixed charges in the film,[36] which in turn should be average concentrations, neglecting their distribution across the film. For a PAH-Os/PVS multilayer in the freshly prepared (reduced) state

$$C_F = [NH_3^+]_{PAH-Os} + [Os(bpy)_2PyCl^+]_{PAH-Os} - [SO_3^-]_{PVS} \tag{4}$$

The effect of the electrolyte concentration on the resulting Donnan potential predicted by eq 2 is shown in Figure 2 calculated for different values of C_F from −0.10 to 0.10 M. Note that the sign of the Donnan potential is only determined by the sign of C_F. At low salt concentrations $C_S \ll |C_F|$, Donnan permselectivity applies, and a linear dependence with a slope of 60 mV per 10-fold in the Galvani potential difference is observed. Under these conditions the film behaves as a cation exchanger ($C_F < 0$ M) or anion exchanger ($C_F > 0$ M) during the redox switching. At high electrolyte concentration ($C_S \gg |C_F|$), Donnan breakdown occurs, and the exchange of salt (anion and cation) takes place.

In order to determine the effect of the acid−base equilibrium over the interfacial Donnan potential, cyclic voltammograms were measured at pH 7.3 in buffer solutions of different ionic strength for films self-assembled from different pH solutions. A typical example is depicted in Figure 3, which shows that the peak potential in voltammograms recorded for a positively capped $(PAH\text{-}Os)_4(PVS)_4PAH\text{-}Os$ film shifts toward more negative values with the increase in salt concentration (as predicted by eq 2 for a film with $C_F > 0$ M). In all experiments

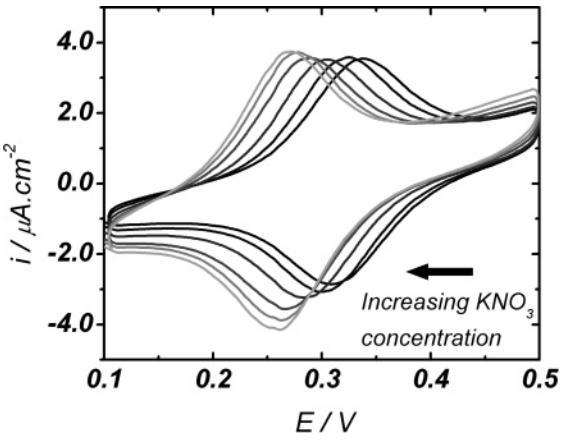

Figure 3. Cyclic voltammograms of $(PAH\text{-}Os)_4(PVS)_4PAH\text{-}Os$ multilayer modified Au electrode self-assembled from PVS and PAH-Os solutions of pH 8.3 and measured in pH 7.3 solutions of different KNO_3 concentrations: 8, 40, 137, 481, 932 and 1500 mM. Sweep rate: 0.025 mV s^{-1}.

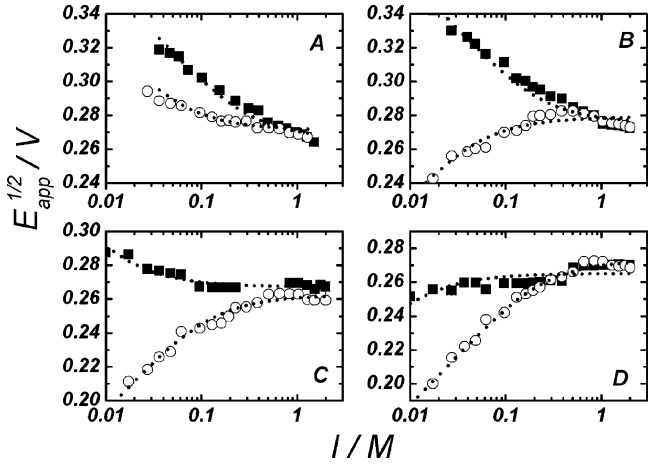

Figure 4. Apparent formal redox potential for ■ $(PAH\text{-}Os)_4(PVS)_4PAH\text{-}Os$ (positively charged capping layer) and ○ $(PAH\text{-}Os)_5(PVS)_5$ (negatively charged capping layer) modified electrodes self-assembled from PAH-Os/PVS solutions of different pH, (A) 8.3, (B) 7.3, (C) 5.5, and (D) 3.5, and measured in pH 7.3 solutions of different KNO_3 concentration, C_S. Dotted lines are best fits with eq 5 (see Table 1 in Supporting Information for best fit parameters).

the apparent redox potential was determined as the average between oxidation and reduction peaks. This is important for voltammograms with a nonzero peak separation, an effect that is particularly noticeable for negatively charge capped multilayers in low ionic strength solutions, due to slow diffusion of charge in the film.[37]

Donnan plots for E^0_{app} vs salt concentration are depicted in Figure 4. Dotted curves show the best fit to the data with the equation resulting from the substitution of eq 2 in eq 1

$$E_{app}^{1/2} = E^0 + \frac{RT}{F}\ln\left[\frac{C_F + (C_F{}^2 + 4C_S{}^2)^{1/2}}{2C_S}\right] \qquad (5)$$

The best fits values for C_F are shown in Figure 6A as a bar plot for easy visualization. From these results it can be observed that for a fixed assembly pH, those films terminated in positively charged PAH-Os always exhibit a greater value for C_F (greater proportion of positive fixed charges) than those capped with negatively charged PVS. The effect of the assembly pH is also noteworthy: For a fixed capping layer, C_F increases monotonically with the increase of adsorption pH. Thus the nature of

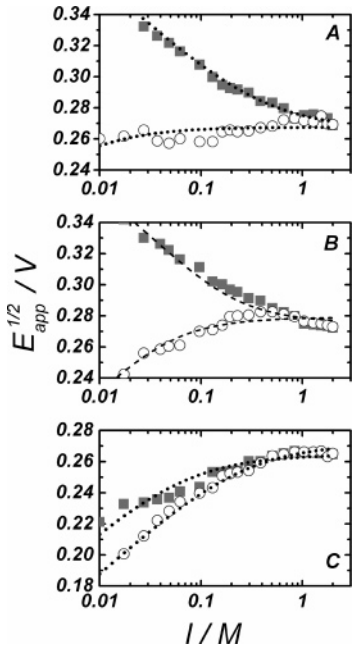

Figure 5. Apparent formal redox potential for ■ $(PAH\text{-}Os)_4(PVS)_4PAH\text{-}Os$ (positively charged capping layer) and ○ $(PAH\text{-}Os)_5(PVS)_5$ (negatively charged capping layer) modified electrodes self-assembled from PAH-Os/PVS solutions of pH 7.3 and measured in solutions of different pH, (A) 4, (B) 7.3, and (C) 10, and KNO_3 concentration. Dotted lines are best fits to eq 5 (see Table 2 in Supporting Information for best fit parameters).

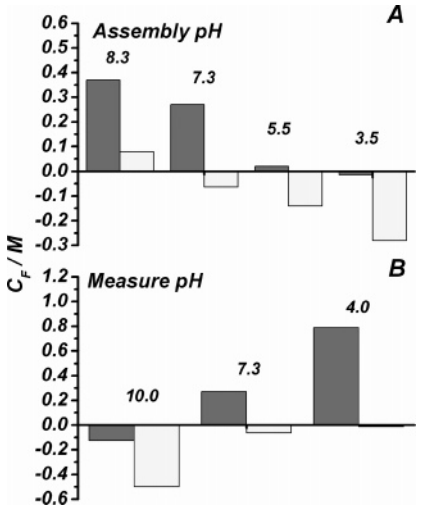

Figure 6. Best fit values of C_F to the data presented in (A) Figure 4 and (B) Figure 5 with eq 5 for $(PAH\text{-}Os)_4(PVS)_4PAH\text{-}Os$ (black bars, positively charged capping layer) and $(PAH\text{-}Os)_5(PVS)_5$ (gray bars, negatively charged capping layer) self-assembled multilayers.

the capping layer not always determines the ionic exchange behavior: Films assembled from pH 8.3 solution always exhibit positive values of C_F while films assembled at pH 3.5 result in negative C_F values. Films assembled between pH 5.5 and 7.3 also follow the general trend, but the sign of C_F depends on the nature of the capping layer. Similar results have been obtained when the polyanion, PVS, was substituted with PAA (Table 1, Supporting Information). The value for E^0 of (271 ± 5) mV (averaged over all the experiments, Tables 1 and 2, Supporting Information) is also in good agreement with 260 mV reported for $Os(bpy)_2ClPyCHO$ in solution.[19]

In order to explain the effect of the adsorption pH and capping layer on the Donnan potential we shall consider two different contributions to the excess of fixed charges, C_F. The first one

TABLE 1: Fraction of Unprotonated Amine Groups, $NH_2/(NH_3^+ + NH_2)$, PAH-Os Molar Content, and Ratios of Fixed Positive Charges ($Os(bpy)_2PyCl^+$and NH_3^+) to Fixed Negative Charges (SO_3^-) Determined from XPS Experiments for $(PAH\text{-}Os)_4(PVS)_4PAH\text{-}Os$ (PAH-Os-Capped) Multilayers Self-Assembled at Different pH

assembly pH	$NH_2/(NH_3^+ + NH_2)$	% PAH-Os	$Os(bpy)_2PyCl^+ + NH_3^+/SO_3^-$	NH_3^+/SO_3^-	$Os(bpy)_2PyCl^+/SO_3^-$
8.3	0.19	52	0.96	0.87	0.09
7.3	0.19	51	0.94	0.86	0.08
5.5	0.03	49	1.01	0.93	0.08
3.5	0.05	48	0.95	0.88	0.07
PAH-Os cast form pH 8.3 solution	0.72				

TABLE 2: Refractive Index (*n*), Extinction Coefficient (*k*), and Steady-State Bilayer Thickness for $(PAH\text{-}Os)_4(PVS)_4PAH\text{-}Os_{4/5}$ Multilayers Assembled at Different pH

assembly pH	*n*	*k*	bilayer thickness/nm
8.3	1.58	0.011	9.7
7.3	1.56	0.011	2.07
5.5	1.56	0.0015	1.2
3.5	1.56	0	1.0

accounts for the effect of the capping layer and is produced by the presence of the topmost layer in contact with the liquid electrolyte. In a three-zone model proposed by Decher,[2] this is a region adjacent to the electrolyte and characterized by an excess of fixed charges compensated by mobile ions. These fixed charges are not strictly located at the electrolyte/film boundary but distributed within a region in the last few layers due to polyelectrolyte interpenetration.[2,38] The existence of this region is inherent to the LbL construction principle and has been widely demonstrated by surface potential measurements.[39−41]

The second contribution to C_F arises from the assembly solution pH. When multilayers built from solutions of different pH are transferred to the measuring solution of pH 7.3, protonation occurs for those films prepared at pH > 7.3 (eq 6a), and deprotonation for those prepared at pH < 7.3 (eq 6b)

$$\text{Pol-NH}_2 + \text{H}^+_{aq} \leftrightarrow \text{Pol-NH}_3^+ \quad (6a)$$

$$[(\text{Pol-NH}_3^+)(\text{PVS-SO}_3^-)] + \text{OH}^-_{aq} \leftrightarrow \text{PVS-SO}_3^- + \text{Pol-NH}_2 + \text{H}_2\text{O} \quad (6b)$$

Note that in both equations a positive or negative fixed charge in the multilayer is created by the uptake of mobile H^+ or OH^- from the electrolyte, respectively. Unlike the effect of the topmost layer, this mechanism is valid for the whole multilayer. It also implies that LbL self-assembled multilayers have a memory effect on the pH of assembly, as will be demonstrated below.

For multilayers containing weak polyelectrolytes, the charge density in the polymer can be changed by the external solution pH after building up the LbL self-assembled structure at a given pH. Therefore cyclic voltammetry experiments were performed in solutions of different pH (4, 7.3, and 10), for films assembled from PAH-Os and PVS solutions of pH 7.3. Figure 5 shows the resulting Donnan plots for E^0_{app} vs salt concentration, and the best fit values for C_F employing eq 5 are depicted in Figure 6B. Here again, films capped with positively charged PAH-Os exhibit larger values of C_F than those finished in negatively capped PVS. For films bearing the same capping layer, C_F decreases with an increase in the measuring solution pH due to film protonation for pH < 7.3 and deprotonation when tested at pH > 7.3. For experiments at pH 7.3 the protonation state of the film remains unchanged, and the sign of C_F is determined by the nature of the topmost assembled layer (symmetric curves in Figure 5B). These results demonstrate that the Donnan potential depends not on the pH of the assembly solution but on the relationship between the pH of assembly and testing solutions, as is predicted by eqs 6a and 6b.

3.2. Effect of the Assembly pH on Ion Exchange. Under Donnan permselectivity, eq 5 predicts that films with positive C_F should behave as anion exchangers and films with negative C_F as cation exchangers. EQCM has been used to study ion exchange in PAH-Os capped films assembled at pH 8.3 and 3.5. We have chosen the number of bilayers in order to have approximately the same osmium coverage in both films: 14.5 bilayers were used for the film assembled at pH 8.3 (high redox charge per bilayer, Figure 10) and 59.5 bilayers for the film assembled at pH 3.5 (low redox charge per bilayer). Areal mass and charge transients were recorded in 0.01 M NaCl solution for an oxidation potential step from 0.10 V (fully reduced state) to 0.60 V (fully oxidized state) followed by a reduction potential step to 0.10 V after 60 s. In EQCM experiments, anion exchangers exchange positive molar masses ($\Delta m/\Delta q$), which result in mass increase during oxidation (anions entering the film) and decrease during reduction (anions leaving the film). On the other hand, for films that exchange cations the opposite behavior is to be expected and thus negative molar masses are exchanged with the external solution.

Figure 7 depicts plots for charge (A) and mass (B) transients

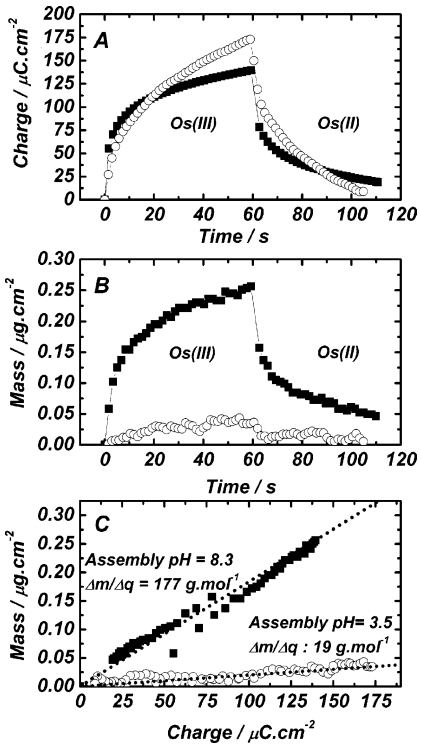

Figure 7. Charge (A) and mass (B) transients and end-to-end mass to charge (C) plot during chronoamperometry of $(PAH\text{-}Os)_n/(PVS)_{n-1}$ multilayers self-assembled from solutions of pH 8.3 (■, $n = 15$) and pH 3.5 (○, $n = 60$) for the oxidation and reduction of the Os(II/III) in 10 mM NaCl from 0.1 to 0.6 V.

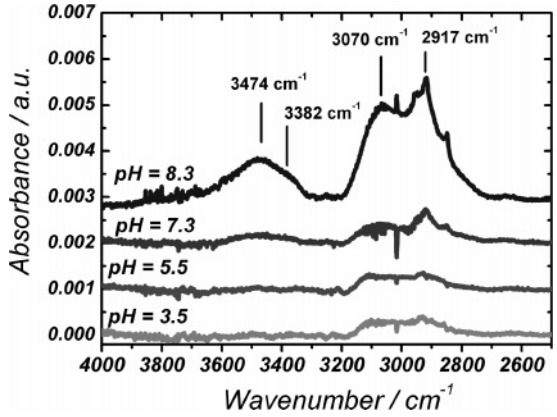

Figure 8. Ex situ FTIR-RAS spectra of $(PAH\text{-}Os)_{15}(PVS)_{14}$ films in air. Incidence angle 80° and reference signal thiolated Au for films assembled from PAH-Os and PVS solutions of different pH as indicated.

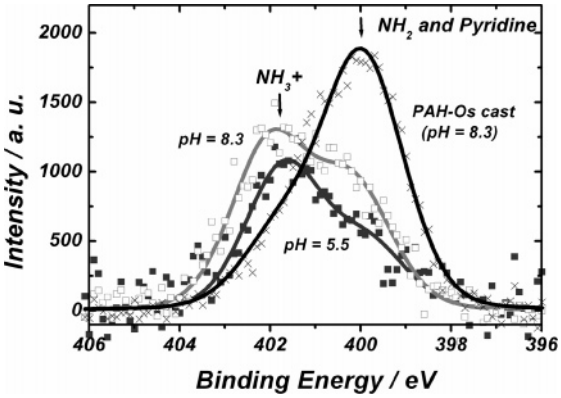

Figure 9. XPS N 1s spectra for a PAH-$[Os(bpy)_2PyCl^+]Cl^-$ cast film on Au (×), and self-assembled $(PAH\text{-}Os)_4(PVS)_4PAH\text{-}Os$ multilayer films from PAH-Os and PVS solutions of pH 8.3 (□) and 5.5 (■).

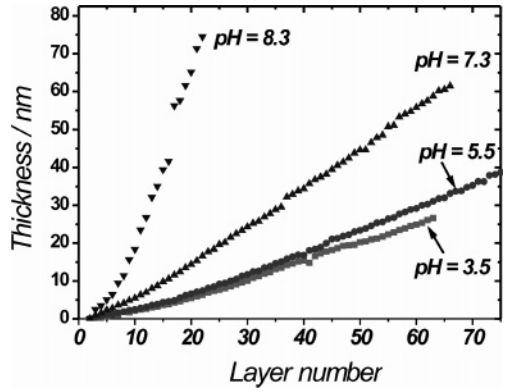

Figure 10. Ellipsometric thickness at 632.9 nm vs number of self-assembled layers for $(PAH\text{-}Os)_n(PVS)_m$ for assembly solutions of indicated pH values.

and end-to-end mass to charge plots (C) for the films assembled at pH 8.3 and 3.5 respectively. While the charge transients (Figure 7A) are similar in shape and intensity for both films, the mass transients (Figure 7B) and the mass-to-charge plot (Figure 7C) show important differences. The film assembled at pH 8.3 behaves as anion exchanger with an apparent exchanged molar mass of 177 g mol^{-1}, which is greater than the molar mass of the anion (Cl^-, *M*r 35.45 g mol^{-1}). This indicates solvent uptake during oxidation and release during reduction as was previously described.[42] On the other hand, the film assembled at pH 3.5 exhibits an exchanged molar mass of 19 g mol^{-1}, smaller than the molar mass of the anion, which suggests that during oxidation/reduction cation exchange compensates charge but its mass is masked by the flux of solvent.

As a conclusion, EQCM experiments demonstrate that the assembly pH could be used to tune ionic permselectivity. This is in agreement with previous experiments carried out by Park et. al[17] with non-redox PAH/PAA cross-linked multilayers, which showed selective permeation of $Fe(CN)_6^{3-}$ or $Ru(NH3)_6^{3+}$ when constructed from basic or acidic solutions, respectively.

3.3. Effect of the Assembly pH on Film Composition and Charge Balance. We have shown that films prepared from solutions of different pH but transferred to a solution of pH 7.3 exhibit different Donnan potentials and ion exchange behavior. This memory effect on the assembly solution pH can be explained on the basis of different populations of protonated/unprotonated amino groups in PAH-Os.

We have used FTIR-RAS and XPS to study the effect of the acid−base equilibrium on the relative populations of NH_2, NH_3^+, SO_3^-, and the Os complex during the adsorption process from solutions of different pH.

Figure 8 shows the FTIR-RAS spectra in the region 4000−2500 cm^{-1} for films assembled at different pH and comprised of 14.5 bilayers. The main difference between the spectra of multilayers assembled from neutral and basic solutions (pH 8.3 and 7.3) and those assembled from acidic (pH 5.5 and 3.3) solutions is the presence in the formers of a broad asymmetric band in the 3600−3300 cm^{-1} spectral region. This band is a convolution of the symmetric and asymmetric N−H stretching bands of the free amino groups expected at ∼3290 cm^{-1} and ∼3350 cm^{-1}, respectively,[17] and the associated water band at 3450 cm^{-1}.[26]

The spectra also show some features which are common to all multilayers: (i) the band centered at 3070 cm^{-1} produced by the overlapping between the asymmetric NH_3^+[10,17,26] and the aromatic C−H stretching modes of pyridine and bypyridine ligands in the osmium complex and (ii) several overlapping bands in the region 3000−2850 cm^{-1} (dominated by a peak at 2917 cm^{-1}), which are typical of methyl and methylene groups stretching modes.[26] These bands are more intense the higher the assembly pH, indicating an increase in the amount of adsorbed polymer.

The quantitative analysis required to calculate the degree of ionization by FTIR is highly complicated by the presence of several overlapping bands[10,11] but is a relatively easy task employing XPS. Figure 9 shows the XPS spectra (not to scale) in the N 1s region for multilayers adsorbed from solutions of pH 8.3 and 5.5 and for PAH-Os cast from a solution of pH 8.3. Two components centered at (400.0 ± 0.2) and (401.8 ± 0.1) eV could be fitted to peaks in the region. The low BE component is associated to the N atoms from the aliphatic NH_2[43] in the PAH-Os backbone and from the N in pyridine and bypyridine ligands in the osmium complex.[44] The second contribution is originated from aliphatic NH_3^+,[43] whose positive charge shifts the peak to higher BEs. The relative amount of each component is dependent on the adsorption pH and for pH 8.3 depends whether the PAH-Os is forming part of a multilayer or not.

In order to quantify the degree of ionization, we first should determine the contribution of pyridine/bypyridine to the low BE peak. This could be accomplished performing the quantification of osmium content and using the structural proportion of five pyridinic N atoms per Os atom present in PAH-Os. Unfortunately it is impossible to obtain good quantification from the osmium peaks due to overlapping with other elements, except in the case of rather thick multilayers where the intensity

of the Au $5p_{3/2}$ peak (overlapping the Os 4f peak) is negligible. We therefore first have determined the molar relationship between total N and osmium from the (thick) PAH-Os cast film and employed this result to calculate the ratio of pyridinic N to total N (0.28), which remains constant for different multilayers because PAH-Os is the only source of nitrogen (N was absent in dry cast PVS films). Then for each different multilayer, we simply determined the pyridinic N from the pyridinic N to total N ratio and the total area of the N 1s peak. A degree of substitution of 1:11.6 (fraction of allylamine segments bearing an attached osmium complex) was also calculated from the total N/Os ratio.

The degrees of ionization for PAH-Os in the multilayers and cast film are reported in Table 1. In agreement with FTIR-RAS results, in the films assembled from solutions of pH 8.3 and 7.3 a fraction (∼20%) of the amino groups are deprotonated, while almost only protonated (95−97%) amino groups exist in multilayers assembled at pH 3.5 and 5.5. As a comparison, degrees of charging in the range 0.7−0.9 were reported for the system PAH/poly(styrene sulfonate) based on similar XPS measurements.[43] Table 1 also indicates that the degree of charging of PAH-Os decreases from 81% in pH 8.3 multilayer to 27% in the cast film. Several examples from this effect are reported in the literature,[10,45−49] showing that the degree of ionization of a weak polyelectrolyte forming part of a multilayer is increased with respect to its solution value due to the presence of an opposite charged polyelectrolyte. While these works reported apparent pK_a values different from the solution counterparts but averaged over all the multilayer, Von Klitzing and Möwald[48] proposed the existence of a proton concentration profile, and hence an apparent pK_a profile, within LbL polyelectrolyte films.

The charge balance in the internal region of LbL multilayers is still an open issue in the literature. Schelenoff[50] has coined the terms "extrinsic" and "intrinsic" to refer to those multilayers where charge balance is achieved with and without the participation of small mobile ions, respectively. Limiting the analysis to multilayers containing PAH, intrinsic charge compensation is supported by direct quantification of infrared active ClO_4^- content by ATR-FTIR.[3] On the other hand, Riegler and Essler[51] suggested that one-third of PAH charges in PAH/poly(styrene sulfonate) films are extrinsically compensated based on ellipsometric and Langmuir−Blodgett isotherms measurements. The presence of mobile ions in multilayers was also supported by X-ray and neutron reflectivity[52] and fluorescence measurements.[40] In an XPS study performed on PAH/PSS multilayers assembled from solutions containing increasing salt concentration,[43] mobile ions were only absent for assembly solutions without added salts. We have performed XPS measurements in the Cl 2p and Na 1s spectral regions in order to determine the type of charge compensation in our system. It is worthwhile to mention that the only small ions present in our PAH-Os and PVS solutions were chloride and sodium ions compensating polyelectrolyte electrostatic charges. The Na 1s peak was absent in all spectra, regardless of the assembly pH. In the case of Cl 2p, a small peak was observed, in quantitative agreement with the stoichiometric amount of chloride present in the osmium complex. It is important to point out that these results imply concentrations of Na^+ and Cl^- bellow the quantitation limit rather than the total absence of these elements, since and mobile ions are necessary to balance the charge of the topmost layer even in an intrinsic charge compensation scenario. XPS results also allow the calculation of the ratio of positive (NH_3^+ + $Os(bpy)_2PyCl^+$) to negative (SO_3^-) fixed charges in the film, which was close to unity in all experiments (Table 1). As a comparison, a similar study performed in poly(butanylviologen)/poly(styrenesulfonate) multilayers exhibited 1:1 stoichiometry and the absence of mobile ions within the film.[53] In other words, the experimental evidence indicates intrinsic charge compensation in multilayers deposited from PAH-Os and PVS solutions without added salts.

While the relative population of free to charged amino groups increases with the adsorption pH, charge balance in the multilayers is intrinsic under all assembly conditions. As a result, those films assembled from basic solutions should exhibit higher molar contents of PAH-Os in order to compensate for its smaller degree of protonation as it is shown in Table 1. These differences in composition are responsible for the differences in the Donnan potentials measured for multilayers prepared from solutions of different pH but tested under identical conditions. In this context it is interesting to point out that in cast or electropolymerized random films, ionic exchange was usually determined by mixing the solution of the redox polymer or electro-polymerizable monomer with a solution of an oppositely charged polyelectrolyte.[54,55] The control of the ion exchange in LbL multilayers by the pH from which PAH-Os is adsorbed modifies the relative composition of the multilayer, producing a similar effect as the former.

In redox polyelectrolyte multilayers the transition from intrinsic polyion−polyion electrostatic compensation to extrinsic polyion-mobile ion interaction can occur by (i) change in the protonation degree of the film by contact with solutions of different pH, (ii) by electrochemical oxidation or reduction thereby introducing extra charge,[56] and (iii) by doping in salt solutions of high ionic strength.[57]

3.4. Effect of the Assembly pH on Film Thickness. The dependence of film thickness with the assembly pH has been described by Rubner et al. for several systems including at least one weak (non-redox) polyelectrolyte.[7,10] We have studied the system PAH-Os/PVS employing ellipsometry and XPS. In ex situ ellipsometric experiments, the ellipsometric angles (Δ and ψ) were measured in different stages of the self-assembly process and fitted under the assumption that the refractive index (n) and extinction coefficient (k) are independent of the number of assembled layers[25] (see Supporting Information for Δ vs ψ plots). In Figure 10, the ellipsometric thickness of the multilayers has been plotted as a function of the dipping cycle number. For each curve, an initial slow film growth is evident in the first few dipping cycles due to the effect of substrate (up to thickness ≈ 7.5 nm), and then a linear growth is observed.

The electrostatic adsorption of the redox polyelectrolyte from PAH-Os solutions of different pH in the range from 3.5 to 8.3 results in quite different film thicknesses as measured by ellipsometry at 632 nm, which grows with the number of dipping cycles more pronounced for PAH-Os solutions of pH above 7, where poly(allylamine) has fewer protonated amino groups. This trend is in agreement with the results reported in previous sections for the redox charge and IR absorbance probed by cyclic voltammetry and FTIR-RAS, respectively. Table 2 compiles the best fit values for n and k and the steady-state bilayer thickness.

These experimental observations can be explained considering the linear charge density of polyelectrolyte chains in the assembly solution. At high pH the linear charge density is small and the polymer adopts coiled conformation (maximum entropy), which in turn promotes high segmental population of loops and tails during adsorption on the surface as reported for $(PAH\text{-}Os)_n(GOx)_n$.[28] At low pHs, a high linear charge density

TABLE 3: Comparison between Ellipsometric Film Thickness Determined from Figure 10 and Thickness Measured from the Intensity of Au 4f Peaks in XPS Experiements for $(PAH\text{-}Os)_4(PVS)_4PAH\text{-}Os$ (PAH-Os-Capped) and $(PAH\text{-}Os)_5(PVS)_5$ (PVS-Capped) Multilayers Self-Assembled at Different pH

assembly pH	capping layer	ellipsometric thickness/nm	XPS thickness/nm
8.3	PAH-Os	23.5	12.5
7.3	PAH-Os	6.3	6.19
5.5	PAH-Os	2.85	3.55
3.5	PAH-Os	2.45	2.58
8.3	PVS	26.8	15.8
7.3	PVS	7.0	7.11
5.5	PVS	3.15	3.36
3.5	PVS	2.49	2.49

in the polyelectrolyte results in an extended rod conformation which is adsorbed flat on the surface.

When compared with previous reports,[10] the growth rate dependence on the assembly pH for PAH-Os/PVS is qualitatively the same as for PAH/PVS. However, a deeper analysis shows that for a given pH, the bilayer thicknesses for PAH-Os/PVS are larger by a factor close to two, probably due to the inclusion of the bulky osmium pyridine−bipyridine complex.

The XPS measurement of the film thickness was performed by analyzing the signal of the underlying Au substrate, which is attenuated by the PAH-Os/PVS multilayer. The decrease in the intensity of the Au 4f photoelectrons with film thickness could be described by the equation[58]

$$\frac{I}{I_0} = \mathrm{e}^{-(d)/(L_{\mathrm{Au}})}$$

where I is the area of Au peak for a multilayer of thickness d, I_0 is the area of the Au peak for the bare Au electrode, and L_{Au} is the effective attenuation length. We have estimated $L_{\mathrm{Au}} = 3.0$ nm from the ellipsometric data for multilayers assembled at pH 7.3. Table 3 shows the comparison of XPS and ellipsometric thickness values for films with 4.5 and 5 assembled layers, respectively. The quantitative agreement between the techniques is excellent for adsorption solution pH 3.5, 5.5, and 7.3, but some discrepancy is found for pH 8.3. Therefore we consider XPS as valid alternative to ex-situ ellipsometry for film thickness determination.

4. Conclusions

We have employed the covalently attached osmium complex in PAH-Os, a weak polyelectrolyte, as an electrochemical probe to study how acid−base equilibrium alters the Donnan potential in LbL-SA PAH-Os/PVS films. Cyclic voltamperometry experiments were performed under different experimental conditions such as the pH and ionic strength of the test electrolyte solution, the pH of the PAH-Os and PVS solutions during film self-assembly, and the nature of charge of the topmost layer.

The peak potential dependence on electrolyte ionic strength was fitted to the Donnan potential equation (eq 5) to yield information on the concentration and sign of fixed ionic charges in the film. These results showed two independent contributions to the Donnan potential, the first arising from the charges introduced by the topmost layer, mainly located in the outer region of the multilayer, and the second one produced by the charges created or destroyed during protonation or deprotonation of the amino groups throughout the film. We have demonstrated that this latter contribution depends on the relationship between the self-assembling and testing pH:

(i) In the case where the testing solution pH < self-assembling pH, protonation of the amines occurs (eq 6a), and the Donnan potential, $\Delta\phi_{\mathrm{D}}$, is positive. EQCM experiments showed a positive exchanged molar mass in excess to the anion molar mass, suggesting the exchange of anions and solvent.

(ii) If the testing solution pH > self-assembling pH, the amines in the film became deprotonated (eq 6b), and the Donnan potential is negative due to an excess of sulfonate groups; thus cations enter the film to compensate for the charge. EQCM experiments showed a positive exchanged molar mass, though smaller than the anion molar mass, which suggests the exchange of both cations and solvent.

(iii) Finally when the testing solution pH ≈ self-assembling pH, the degree of protonation of amines in the film remains unchanged and the Donnan potential is determined by the excess charge in the polyelectrolyte capping layer.

The proposed mechanism requires that the freshly self-assembled multilayers have memory of their assembly solution pH, based on the degree of protonation of the amines in PAH-Os and the PAH-Os to PVS molar ratio as has been proved by XPS and FTIR-RAS measurements.

As a concluding remark, we have demonstrated that acid−base equilibrium in layer-by-layer self-assembled polyelectrolyte films has a profound impact on the Donnan potential. On the basis of several experimental techniques, we have provided a detailed description of the mechanisms involved and have shown how the effect can be used to control the ionic exchange in redox active multilayers. Work is in progress to assess the validity of the Donnan model for thin ($d \approx 1/\kappa_{\mathrm{DB}}$) redox polyelectrolyte films.

Acknowledgment. The authors are grateful to CONICET, University of Buenos Aires, and ANPCyT (BID 1728 OC-AR PICT 2003 No. 06-17170) for financial support. M.T. acknowledges a cooperative industrial research doctoral fellowship from CONICET and FUDETEC. E.J.C. and F.W. are fellows of CONICET.

Supporting Information Available: Best fit values of C_{F} and E^0 obtained with eq 5 for PAH-Os/PVS and PAH-Os/PAA multilayers self-assembled and tested at different pH, plot of ellipsometric angles ψ vs Δ for different number of dipping cycles in PAH-Os and PVS solutions of different pH, and derivation of eq 2. This material is available free of charge via the Internet at http://pubs.acs.org.

References and Notes

(1) Decher, G. *Science* **1997**, *277*, 1232.
(2) Decher, G. Polyelectrolyte multilayers, an overview. In *Multilayer Thin Films*; Decher, G., Schlenoff, B. J., Eds.; Wiley-VCH: Weinheim, Germany, 2003.
(3) Jaber, J. A.; Schlenoff, J. B. *J. Am. Chem. Soc.* **2006**, *128*, 2940.
(4) Dubas, S. T.; Schlenoff, J. B. *Macromolecules* **1999**, *32*, 8153.
(5) Arys, X.; Jonas, A. M.; Laschewsky, A.; Legras, R. Supramolecular polyelectrolyte assemblies. In *Supramolecular Polymers*; Ciferri, A., Ed.; Marcel Dekker: New York, 2000.
(6) Fery, A.; Schöler, B.; Cassagneau, T.; Caruso, F. *Langmuir* **2001**, *17*, 8779.
(7) Shiratori, S. S.; Rubner, M. F. *Macromolecules* **2000**, *33*, 4213.
(8) Yoo, D.; Shiratori, S. S.; Rubner, M. F. *Macromolecules* **1998**, *31*, 4309.
(9) Durstock, M. F.; Rubner, M. F. *Langmuir* **2001**, *17*, 7865.
(10) Choi, J.; Rubner, M. F. *Macromolecules* **2005**, *38*, 116.
(11) Itano, K.; Choi, J.; Rubner, M. F. *Macromolecules* **2005**, *38*, 3450.
(12) Zhai, L.; Nolte, A. J.; Cohen, R. E.; Rubner, M. *Macromolecules* **2004**, *37*, 6113.
(13) Burke, S. E.; Barrett, C. J. *Macromolecules* **2004**, *37*, 5375.
(14) Chung, A. J.; Rubner, M. F. *Langmuir* **2002**, *18*, 1176.

(15) Rmaile, H. H.; Farhat, T. R.; Schlenoff, J. B. *J. Phys. Chem. B* **2003**, *107*, 14401.
(16) Antipova, A. A.; Sukhorukova, G. B. *Adv. Colloid Interface Sci.* **2004**, *111*, 49.
(17) Park, M.-K.; Deng, S.; Advincula, R. C. *J. Am. Chem. Soc.* **2004**, *126*, 13723.
(18) Kang, E.-H.; Liu, X.; Sun, J.; Shen, J. *Langmuir* **2006**, *22*, 7894.
(19) Calvo, E. J.; Wolosiuk, A. *J. Am. Chem. Soc.* **2002**, *124*, 8490.
(20) Danilowicz, C.; Corton, E.; Battaglini, F. *J. Electroanal. Chem.* **1998**, *445*, 89.
(21) Hodak, J.; Etchenique, R.; Singhal, K.; Bartlett, P. N.; Calvo, E. J. *Langmuir* **1997**, *13*, 2708.
(22) Finklea, H. O.; Snider, D. A.; Fedyk, J. *Langmuir* **1990**, *6*, 371.
(23) Calvo, E.; Danilowicz, C.; Etchenique, R. *J. Chem. Soc., Faraday Trans.* **1995**, *91*, 4083.
(24) Calvo, E. J.; Forzani, E.; Otero, M. *J. Electroanal. Chem.* **2002**, *538/539*, 231.
(25) Forzani, E. S.; Otero, M.; Perez, M. A.; Teijelo, M. L.; Calvo, E. J. *Langmuir* **2002**, *18*, 4020.
(26) Bonazzola, C.; Calvo, E. J.; Nart, F. *Langmuir* **2003**, *19*, 5279.
(27) Scofield, J. H. *J. Electron Spectrosc.* **1976**, *8*, 129.
(28) Flexer, V.; Forzani, E. S.; Calvo, E. J.; Luduenã, S. J.; Pietrasanta, L. I. *Anal. Chem.* **2006**, *78*, 399.
(29) Naegeli, R.; Redepening, J.; Anson, F. C. *J. Phys. Chem.* **1986**, *20*, 6227.
(30) Ugo, P.; Anson, F. C. *Anal. Chem.* **1989**, *61*, 1799.
(31) Doblhofer, K.; Armstrong, R. D.; Asturias, G. E.; Jang, G.; MacDiarmid, A. G.; Zhong, C. *Ber. Bunsen-Ges. Phys. Chem.* **1991**, *11*, 1381.
(32) Doblhofer, K.; Vorotyntsev, M. Chapter 3. In *Electroactive Polymer Electrochemistry. Part 1. Fundamentals*; Lyons, M. E. G., Ed.; Plenum Press: New York, 1994; pp 375.
(33) Redepenning, J.; Tunison, H. M.; Finklea, H. O. *Langmuir* **1993**, *9*, 1404.
(34) Calvo, E. J.; Schiffrin, D. J. *J. Electroanal. Chem.* **1984**, *163*, 257.
(35) Ohshima, H.; Ohki, S. *Biophys. J.* **1985**, *47*, 673.
(36) English, A. E.; Mafé, S.; Manzanares, J. A.; Yu, X.; Grosberg, A. Y.; Tanaka, T. *J. Chem. Phys.* **1996**, *104*, 8713.
(37) Tagliazucchi, M.; Calvo, E. J. *J. Electroanal. Chem* **2007**, *599*, 249.
(38) Castelnovo, M.; Joanny, J. F. *Langmuir* **2000**, *16*, 7524.
(39) Schwarz, B.; Schönhoff, M. *Langmuir* **2002**, *18*, 2964.
(40) Caruso, F.; Lichtenfeld, H.; Donath, E.; Möhwald, H. *Macromolecules* **1999**, *32*, 2317.
(41) Ladam, G.; Schaad, P.; Voegel, J. C.; Schaaf, P.; Decher, G.; Cuisinier, F. *Langmuir* **2000**, *16*, 1249.
(42) Tagliazucchi, M.; Grumelli, D.; Bonazzola, C.; Calvo, E. J. *J. Nanosci. Nanotechnol.* **2006**, *6*, 1731.
(43) Lourenco, J. M. C.; Ribeiro, P. A.; Rego, A. M. B. d.; Fernandes, F. M. B.; Outinho, A. M. C.; Raposo, M. *Langmuir* **2004**, *20*, 8103.
(44) Cohen, M. R.; Merrill, R. P. *Surf. Sci.* **1991**, *245*, 1.
(45) Xie, A. F.; Granick, S. *Macromolecules* **2002**, *35*, 1805.
(46) Xie, A. F.; Granick, S. *J. Am. Chem. Soc.* **2001**, *123*, 3175.
(47) Petrov, A. I.; Antipov, A. A.; Sukhorukov, G. *Macromolecules* **2003**, *36*, 10079.
(48) Klitzing, R. v.; Möwald, H. *Langmuir* **1995**, *11*, 3554.
(49) Rmaile, H. H.; Schlenoff, J. B. *Langmuir* **2002**, *18*, 8263.
(50) Schlenoff, J. B.; Ly, H.; Li, M. *J. Am. Chem. Soc.* **1998**, *120*, 7626.
(51) Riegel, H.; Essler, F. *Langmuir* **2002**, *18*, 6694.
(52) Schmitt, J.; Grünewald, T.; Decher, G.; Pershan, P. S.; Kjaer, K.; Lösche, M. *Macromolecules* **1993**, *26*, 7058.
(53) Laurent, D.; Schlenoff, J. B. *Langmuir* **1997**, *13*, 1552.
(54) Ostrom, G. S.; Buttry, D. A. *J. Phys. Chem.* **1995**, *99*, 15236.
(55) Barbero, C.; Miras, M. C.; Haas, O.; Kötz, R. *J. Electrochem. Soc.* **1997**, *144*, 4170.
(56) Grumelli, D. E.; Garay, F.; Barbero, C. A.; Calvo, E. J. *J. Phys. Chem. B* **2006**, *110*, 15345.
(57) Farhat, T. R.; Schlenoff, J. B. *J. Am. Chem. Soc.* **2003**, *125*, 4627.
(58) Petrovykh, D. Y.; Kimura-Suda, H.; Tarlov, M. J.; Whitman, L. J. *Langmuir* **2004**, *20*, 429.